Physica B 608 (2021) 412897

Contents lists available at ScienceDirect

Physica B: Physics of Condensed Matter

journal homepage: http://www.elsevier.com/locate/physb

First-principles study for comparison of the electronic and optic bandgaps of the $CH_3NH_3Pb_{1-x}Y_xI_3$ (Y=Bi, x=0.00, 0.125) and $CH_3NH_3Pb_{1-x}Y_xI_3$ (Y=Ca, Sr, x=0.125, 0.250) perovskites

C. Soykan [a,*], H. Gocmez [b]

[a] Vocational School of Health Services, Ahi Evran University, Kırşehir, Turkey
[b] Department of Metallurgy and Materials Engineering, Dumlupınar University, Kütahya, Turkey

ARTICLE INFO

Keywords:
Halid perovskite $CH_3NH_3Pb_{(1-x)}Y_{(x)}I_3$ (Y=Bi, Sr,Ca)
Density functional theory
Optical and electronic properties
Absorption coefficient
Tauc method

ABSTRACT

We computed the optical bandgaps of the $CH_3NH_3Pb_{(1-x)}Y_{(x)}I_3$ (Y=Bi, x = 0.00, 0.125) and $CH_3NH_3Pb_{(1-x)}Y_{(x)}I_3$ (Y=Ca, Sr, x = 0.125, 0.250) perovskite crystal structures using optical arguments such as the imaginary part of the dielectric function $\varepsilon_2(\omega)$, absorption coefficient (α), the zero-crossing point of the $(\alpha h\upsilon)^2$ versus $(h\upsilon)$. Density Functional Theory (DFT) calculations and the Vienna ab-initio simulation package (VASP) are used in theoretical calculations. The optical bandgap of the stoichiometric $CH_3NH_3PbI_3$ phase calculated as 1.694 eV is in agreement with both experimental and theoretical studies. The optical bandgaps of the non-stoichiometric phases are calculated as 1.358 eV, 1.493 eV, 1.537 eV, 1.503 eV, and 1.588 eV, respectively. These optical bandgaps results are reported for the first time in this study.

1. Introduction

The hybrid lead-based halide perovskite crystal structures are seen as suitable candidates with increasing efficiency for solar cells. Therefore, both experimental and theoretical studies on the structural and electronic properties of $MAPbI_3$ perovskite crystal structures are continuing intensively. When the literature is examined, especially in theoretical studies, while calculating the electronic bandgap of perovskite materials based on the interactions of valence electrons by using electronic arguments (or data) such as the density of state (DOS), partial density of state (pDOS), and electronic band distribution; on the other hand, optical bandgaps are analyzed by using optical arguments (or data) such as dielectric function, absorption coefficient, Tauc method. At this point, it becomes important to compare the calculated electronic band gaps with the optical band gaps.

Recently, studies on electronic bandgaps of the $CH_3NH_3Pb_{(1-x)}Y_{(x)}I_3$ (Y=Bi, Ca,Sr, x = 0.00, 0.125, 0.250, 0.500, 0.750, 1.000) perovskite crystal phases were mentioned in detail in our previous studies [1,2]. Additionally, it is available in experimental and theoretical studies to obtain optical bandgaps using optical arguments (or data) for $MAPbI_3$ lead-based halide perovskite crystal structures. In this study, available experimental and theoretical studies on the optical bandgap calculated using only optical arguments (or data) such as dielectric function, absorption coefficient, reflectance, ultraviolet photoelectron spectroscopy (UPS), and UV–visible spectroscopy for the $CH_3NH_3Pb_{(1-x)}Y_{(x)}I_3$ (Y=Bi, Ca, Sr, x = 0.00, 0.125, 0.250, 0.500, 0.750, 1.000) crystal structures will be reported.

The optical bandgap and the maximum point of the valence band in the perovskite $CH_3NH_3PbI_3$ crystal were determined by the reflectance and ultraviolet photoelectron spectroscopy (UPS) method by Kim et al. [3]. The optical bandgap of $(CH_3NH_3)PbI_3$ perovskite crystal is investigated by using the UV–Visible spectroscopy method by Baikie et al. [4]. The determined optical bandgap in this study is compared with the electronic bandgap [4]. The near band-edge optical responses of solution-processed $CH_3NH_3PbI_3$ perovskite structure on mesoporous TiO_2 for mesoscopic heterojunction solar cells are studied by Photoluminescence (PL) by Yamada et al. [5]. In Yamada study, at room temperature, the $(F(R)\alpha h\upsilon)^2$ versus $h\upsilon$ spectrum shows that the extrapolated lines's zero-crossing point (x-intercept) is 1.59 eV. Also, PL and PL excitation (PLE) spectrum shows that the bandgap energy exceeds 1.60 eV and 1.64 eV, respectively [5]. Also, in Dang et al. study, the optical bandgap of $CH_3NH_3PbI_3$ single crystal is determined as 1.48 eV by using the UV–vis spectrum [6]. Finally, the $CH_3NH_3Pb_{(1-x)}Pd_{(x)}I_3$ crystal structure at x = 0.00, 0.125, 0.250, 0.500, 0.750, 1.000 ratios was synthesized by Navas et al. [7]. For the samples is obtained the UV–vis spectra and Tauc plots are obtained from the spectra measured.

* Corresponding author.
E-mail address: cengiz.soykan@ahievran.edu.tr (C. Soykan).

https://doi.org/10.1016/j.physb.2021.412897
Received 26 November 2020; Received in revised form 31 January 2021; Accepted 9 February 2021
Available online 12 February 2021

Table 1
The calculated optical bandgaps of the $CH_3NH_3Pb_{(1-x)}Y_{(x)}I_3$ (Y=Bi, x = 0.00, 0.125) and $CH_3NH_3Pb_{(1-x)}Y_{(x)}I_3$ (Y=Ca, Sr, x = 0.125, 0.250) perovskite crystal structures and the other comparable experimental-theoretical data.

Structure	Method	Bandgaps		Directions	Ref.
		$E_{elect-g}(eV)$	$E_{opt-g}(eV)$[a]	Direct or Indirect	
$CH_3NH_3PbI_3$	Our cal.	1.682	1.694	$R \rightarrow R$ Direct	
	Other cal.		1.540	$\Gamma \rightarrow \Gamma$ Direct	[7]
	Exp.		1.550	Direct	[3]
			1.510		[4]
			1.600–1.640	Direct	[5]
			1.480	Direct	[6]
$CH_3NH_3Pb_{0.875}Bi_{0.125}I_3$	Our cal.	1.306	1.358	$\Gamma \rightarrow \Gamma$ Direct	
$CH_3NH_3Pb_{0.875}Ca_{0.125}I_3$	Our cal.	1.440	1.493	$\Gamma \rightarrow \Gamma$ Direct	
$CH_3NH_3Pb_{0.750}Ca_{0.250}I_3$	Our cal.	1.540	1.537	$\Gamma \rightarrow \Gamma$ Direct	
$CH_3NH_3Pb_{0.875}Sr_{0.125}I_3$	Our cal.	1.525	1.503	$\Gamma \rightarrow \Gamma$ Direct	
$CH_3NH_3Pb_{0.750}Sr_{0.250}I_3$	Our cal.	1.619	1.588	$\Gamma \rightarrow \Gamma$ Direct	

[a] In this study, optical bandgaps $E_{opt-g}(eV)$ calculated using only optical arguments from other previous theoretical and experimental studies are referred to. These calculated or observed optical bandgaps are compared with the data of crystal structures with the most suitable electronic bandgaps for solar cells that we calculated in our previous studies [1,2].

The optical bandgap at x = 0.00 ratio (for $CH_3NH_3PbI_3$) are determined as 1.54 eV [7].

Our main goal is to calculate the optical bandgap using absorption coefficient data and the Tauc method for combinations that give the most suitable electronic bandgap by using the density of state and electronic band distribution calculation for solar cells calculated in our previous studies [1,2]. Because, when the literature is examined, the importance of comparing the electronic bandgap and the optical bandgap in the studies that design photo absorber material for solar cells is seen. Also, while many experimental and theoretical studies calculate optical bandgaps for $CH_3NH_3PbI_3$ structure [4–7], to the best of our knowledge, the optical bandgaps of the nonstoichiometric $CH_3NH_3Pb_{(1-x)}Bi_{(x)}I_3$ (x = 0.00, 0.125) and $CH_3NH_3Pb_{(1-x)}Y_{(x)}I_3$ (Y=Ca, Sr, x = 0.125, 0.250) perovskite structures that we have calculated electronic bandgaps in our previous studies will be reported for the first time in this study [1,2].

2. Computational method

All total-energy calculations are performed with the Vienna ab-*initio* simulation package (VASP), based on the Density Functional Theory (DFT) using the Projector Augmented Wave (PAW) method developed by Blöchl to calculate the electronic structure of materials [8–16]. To describe the exchange-correlation functional used the generalized gradient approximation (GGA) was developed by Perdew, Burke, and Enrzerhof (PBE) [17].

In our previous study, structural and electronic properties at x ratios were calculated for $CH_3NH_3Pb_{(1-x)}Bi_{(x)}I_3$ (x = 0.00 0.125, 0.250, 0.500, 0.750, and 1.00) perovskite crystal structures [1]. According to our results, it was determined that the $CH_3NH_3Pb_{0.875}Bi_{0.125}I_3$ crystal phase formed with x = 0.125 ratios has the most suitable electronic bandgap (1.30 eV) for solar cells. Full details of the structural and electronic calculations (related to the electronic bandgap) for the $CH_3NH_3Pb_{0.875}Bi_{0.125}I_3$ phase are given in our previous study [1].

Similarly, in other our previous study, structural and electronic properties at x = 0.125, 0.250, 0.500, 0.750, and 1.00 ratios were calculated for the $CH_3NH_3Pb_{(1-x)}Y_{(x)}I_3$ (Y=Ca,Sr) perovskite structures [2]. The electronic bandgaps for $CH_3NH_3Pb_{(1-x)}Ca_{(x)}I_3$ (x = 0.125, 0.250) crystal structure were calculated as 1.44 eV (x = 0.125) and 1.54 eV (x = 0.250), respectively. Also, the electronic bandgaps for $CH_3NH_3Pb_{(1-x)}Sr_{(x)}I_3$ (x = 0.125, 0.250) crystal structure were calculated as 1.525 eV (x = 0.125) and 1.619 eV (x = 0.250), respectively [2]. The structural and electronic (especially related to electronic bandgaps) details about these calculations are given in the previous study [2].

In this study, according to the results of our previous studies, optical bandgaps were calculated by using the optical absorption coefficient data calculated depending on the frequency in the $CH_3NH_3Pb_{(1-x)}Bi_{(x)}I_3$ (x = 0.00, 0.125) and $CH_3NH_3Pb_{(1-x)}Y_{(x)}I_3$ (Y=Ca, Sr x = 0.125, 0.250) perovskite crystal structures with the most suitable electronic bandgap for solar cells [1,2].

It is very important to determine the behavior of the imaginary part of the dielectric function $\varepsilon_2(\omega)$ in determining the optical properties of any material. To obtain the imaginary part of the full (electronic and ionic) frequency-dependent dielectric function $\varepsilon_2(\omega)$, we have calculated the steps given below separately.

- Step 1. A standard DFT calculation has been made,
- Step 2. The electronic contributions to the frequency-dependent dielectric function $\varepsilon(\omega)$ have been calculated.
- Step 3. The ionic contributions to the frequency-dependent dielectric function $\varepsilon(\omega)$ have been calculated.
- Step 4. Two the frequency-dependent dielectric function $\varepsilon(\omega) = \varepsilon_{elec}(\omega) + \varepsilon_{ion}(\omega)$ combined.

In the calculation of electronic contributions to the frequency-dependent dielectric function $\varepsilon(\omega)$ (step 2) are used LEOPTICS = .TRUE.-tag. In step 3, the ionic contributions to the frequency-dependent dielectric function were calculated using IBRION = 8-tag and LEPSILON = .TRUE.-tag. Finally, in the fourth step, the vasprun.xml file obtained from the calculation made by considering both electronic and ionic contributions to the dielectric function $\varepsilon(\omega)$ was used to create the imaginary part of the full frequency-dependent dielectric function $\varepsilon_2(\omega)$ and the absorption coefficient data (α, cm^{-1}) with the sumo code [18].

To ensure that our calculations are in harmony with the electronic bandgap calculations we obtained in our previous studies, the energy cutoff value was chosen the same as the previous ones [1,2]. The selected kinetic energy cutoff values for $CH_3NH_3PbI_3$ (x = 0.00), $CH_3NH_3Pb_{0.875}Bi_{0.125}I_3$ (x = 0.125), and $CH_3NH_3Pb_{(1-x)}Y_{(x)}I_3$ (Y=Ca, Sr, x = 0.125, 0.250) perovskite crystal structures are 600 eV, 500 eV, and 500 eV, respectively. Also, Monshorst-Pack special points mesh with a size 4 × 4x4 has been selected for all calculations [19]. Besides, the energy convergence criterion of the electronic self-consistency was chosen as 10^{-8} eV/atom.

The absorption coefficient data (α, cm^{-1}) against energy (hυ, eV) were obtained using the sumo code [18]. It is well known that the relationship between the optical bandgap and the absorption coefficient is given as follows [20]:

$$\alpha h\upsilon = b(h\upsilon - E_{opt-g})^{1/2} \quad (1)$$

where α is the optical absorption coefficient, h is the Plank's constant, b

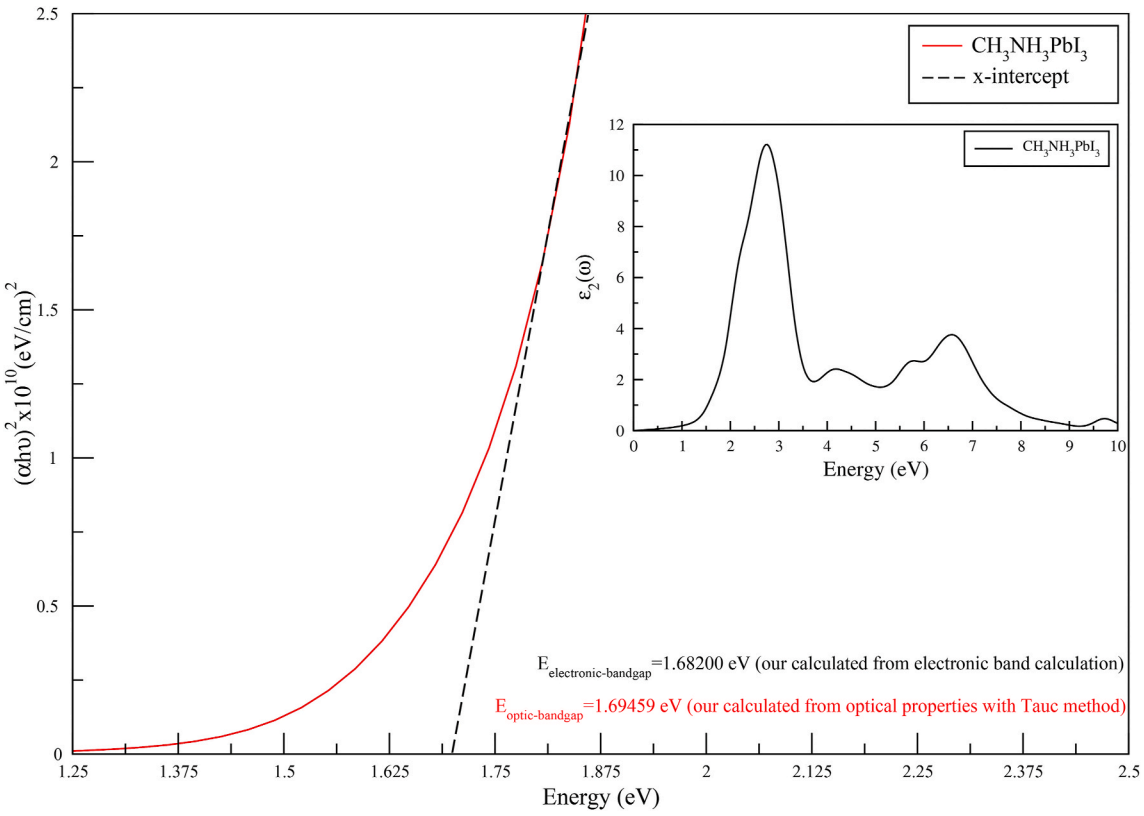

Fig. 1. The Tauc plot obtained using the zero-crossing point of the $(\alpha h\upsilon)^2$ versus $(h\upsilon)$. The right inset shows the imaginary part of the dielectric function $\varepsilon_2(\omega)$ in the stoichiometric $CH_3NH_3PbI_3$ phase.

is a constant for a direct band transition, υ is the radiation frequency, and E_{opt-g} is the optical bandgap. The 1/2 power given in Eq. (1) indicates that the band transitions of all crystal phases studied in this study are direct (Γ→Γ or R→R). The optical bandgap (E_{opt-g}) is obtained from the intercept of $(\alpha h\upsilon)^2$ versus photon energy $(h\upsilon)$ by the Tauc method. We determined the optical bandgap of the $CH_3NH_3PbI_3$ (x = 0.00), $CH_3NH_3Pb_{0.875}Bi_{0.125}I_3$ (x = 0.125), and $CH_3NH_3Pb_{(1-x)}Y_{(x)}I_3$ (Y=Ca, Sr, x = 0.125, 0.250) perovskite crystal structures using this method.

3. Results and discussion

In this study, to calculate the optical bandgaps (E_{opt-g}) of $CH_3NH_3PbI_3$, $CH_3NH_3Pb_{0.875}Bi_{0.125}I_3$, $CH_3NH_3Pb_{0.875}Ca_{0.125}I_3$, $CH_3NH_3Pb_{0.750}Ca_{0.250}I_3$, $CH_3NH_3Pb_{0.875}Sr_{0.125}I_3$, and $CH_3NH_3Pb_{0.750}Sr_{0.250}$ I_3 crystal structures, firstly, we calculated the imaginary parts of the dielectric functions $\varepsilon_2(\omega)$ for all the crystal structures. $\varepsilon_2(\omega)$ is very useful in determining the optical properties of materials. Because the interaction of a photon and electrons in crystal structures can be described from the ground-state electronic states. The electric field of the photon, which interacts with the electrons of the crystal system, is responsible for the optical transitions between occupied and unoccupied states. The joint density of states between the valence and the conduction band in a system excited by a photon will give the spectrum that occurred from the excited states. Also, the absorption spectra can be calculated directly from the imaginary part of the dielectric function $\varepsilon_2(\omega)$ computed for crystal structures. From the calculated $\varepsilon_2(\omega)$ for all crystal structures, we calculated the absorption coefficient (cm^{-1}) versus energy (eV) by using the sumo code [18]. However, the absorption coefficient (cm^{-1}) - energy (eV) graphs are not shown in this study. Next, the optical bandgaps (E_{opt-g}) were obtained from the intercept of $(\alpha h\upsilon)^2$ versus photon energy $(h\upsilon)$ by using extrapolation (x-intercept) with the Tauc method.

The calculated optical bandgaps are given in Table 1 to compare with other theoretical and experimental studies. Focusing on Table 1, there is a 0.71% difference between the electronic bandgap ($E_{elect-g}$) calculated as 1.682 eV ($R \rightarrow R$ Direct) in our previous studies for the $CH_3NH_3PbI_3$ perovskite structure and the optical bandgap (E_{opt-g}) calculated as 1.694 eV in this study [1,2]. This result shows that the calculated electronic bandgap ($E_{elect-g}$) is quite compatible with the calculated optical bandgap (E_{opt-g}). When this situation is evaluated in terms of other theoretical and experimental optical bandgaps studies, it differs by 9.29%, 12.18%, 5.87–3.29%, 14.46%, and 10%, respectively, with optical bands of 1.550 eV [3], 1.510 eV [4], 1.600–1.640 eV [5], 1.480 eV [6], and 1.540 eV [7]. It is seen that there is an agreement between the calculated optical band gap and other experimental and theoretical studies at acceptable limits. The highest difference is with the study calculated as 12.18% and 1.51 eV [4]. We think that the difference seen with other studies is due to the difference in calculation and observation conditions.

When we focus on the non-stoichiometric $CH_3NH_3Pb_{0.875}Bi_{0.125}I_3$, $CH_3NH_3Pb_{0.875}Ca_{0.125}I_3$, $CH_3NH_3Pb_{0.750}Ca_{0.250}I_3$, $CH_3NH_3Pb_{0.875}Sr_{0.125}$ I_3, and $CH_3NH_3Pb_{0.750}Sr_{0.250}I_3$ perovskite crystal structures presented in Table 1, the electronic band gaps calculated in our previous studies [1,2] and the optical band gaps calculated in this study seem to be in perfect agreement. The difference between the calculated electronic ($E_{elect-g}$) and optical bandgaps (E_{opt-g}) of $CH_3NH_3Pb_{0.875}Bi_{0.125}I_3$, CH_3NH_3 $Pb_{0.875}Ca_{0.125}I_3$, $CH_3NH_3Pb_{0.750}Ca_{0.250}I_3$, $CH_3NH_3Pb_{0.875}Sr_{0.125}I_3$, and $CH_3NH_3Pb_{0.750}Sr_{0.250}I_3$ crystal structures is approximately 3.83%, 3.55%, 0.19%, 1.46%, and 1.95%, respectively. To the best of our knowledge, there are no experimental or theoretical studies on the optical band gaps of non-stoichiometric $CH_3NH_3Pb_{0.875}Bi_{0.125}I_3$, $CH_3NH_3Pb_{0.875}Ca_{0.125}I_3$, $CH_3NH_3Pb_{0.750}Ca_{0.250}I_3$, $CH_3NH_3Pb_{0.875}$ $Sr_{0.125}I_3$, and $CH_3NH_3Pb_{0.750}Sr_{0.250}I_3$ phases. Therefore, these data are reported for the first time in this study.

Fig. 1 presents the imaginary part of the dielectric function $\varepsilon_2(\omega)$ of

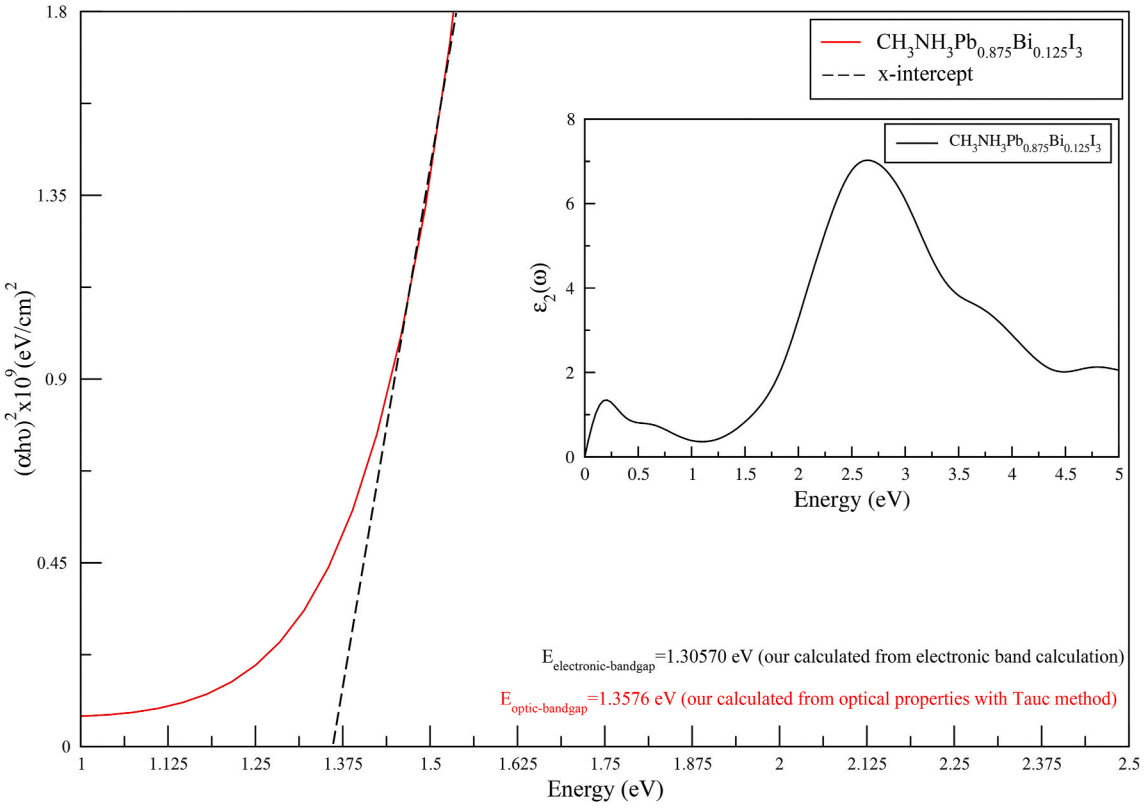

Fig. 2. The Tauc plot obtained using the zero-crossing point of the $(\alpha h\nu)^2$ versus $(h\nu)$. The right inset shows the imaginary part of the dielectric function $\varepsilon_2(\omega)$ in the non-stoichiometric $CH_3NH_3Pb_{0.875}Bi_{0.125}I_3$ phase.

$CH_3NH_3PbI_3$ perovskite crystal structure and the $(\alpha h\nu)^2$ versus photon energy $(h\nu)$ by using extrapolation (x-intercept) with the Tauc method. If we first focus on the behavior of the imaginary part of the dielectric function $\varepsilon_2(\omega)$ in Fig. 1, the initial range of the largest peak corresponds approximately to the region of 1–1.8 eV. This behavior is evidence supporting the behavior of the $(\alpha h\nu)^2$ statement in Fig. 1. However, to calculate the optical band gap more accurately, the $(\alpha h\nu)^2$ versus photon energy $(h\nu)$ graph has been zoomed in the 1–2 eV region. The zero-crossing point was calculated as 1.694 eV by applying linear interpolation for the $CH_3NH_3PbI_3$ structure. in Fig. 1, The dashed line indicates linear extrapolation (x-intercept). The calculated optical bandgap as 1.694 eV for the $CH_3NH_3PbI_3$ crystal structure is highly consistent with both experimental and theoretical optical bandgaps previously reported [3, 4, 5, 6 7]. Also, it is highly compatible with the electronic bandgap we calculated in our previous studies. The difference is only 0.71% [1, 2].

In Fig. 2, the change of the imaginary part of the dielectric function $\varepsilon_2(\omega)$ and the $(\alpha h\nu)^2$ term for the $CH_3NH_3Pb_{0.875}Bi_{0.125}I_3$ structure, which is formed by doping Bi^{3+} ions at x = 0.125 ratios to $CH_3NH_3Pb_{(1-x)}Bi_{(x)}I_3$ perovskite structure, according to the excitation photon energy $(h\nu)$ is presented. Focusing on Fig. 2, there is a small peak in the range from 0 to 0.25 eV in the imaginary part of the dielectric function $\varepsilon_2(\omega)$. However, the starting point of the largest peak is 1.25 eV. The peak that started to rise above 1.25 eV is settled between 1.25 eV and 2.75 eV. With the maximum peak rising from 1.25 eV in the imaginary part of the dielectric function $\varepsilon_2(\omega)$, the behavior of the term $(\alpha h\nu)^2$ in response to energy $(h\nu)$ is similar. Therefore, the optical band gap value calculated by zero-crossing point extrapolation (x-intercept) can be trusted. the zero-crossing point value calculated as 1.358 eV by using the extrapolation (x-intercept) process. This is the optical band gap value of the crystal phase. It is compatible with the 1.306 eV electronic bandgap that we calculated in our previous study [1]. The difference is approximately 3.82%.

Similarly, the optical bandgaps of the $CH_3NH_3Pb_{0.875}Ca_{0.125}I_3$, $CH_3NH_3Pb_{0.750}Ca_{0.250}I_3$ phases were calculated in Fig. 3 a) and Fig. 3 b), respectively. When we focus on Fig. 3 a), two high peaks can be seen in the imaginary part of the dielectric function $\varepsilon_2(\omega)$, which are located approximately 3 eV and 6.5 eV. The peak that reaches a maximum value of around 3 eV is higher than these peaks. The initial value of this peak is in the region 1–1.6 eV. The zero-crossing point of the curve showing the behavior of the term $(\alpha h\nu)^2$ versus the excitation photon energy $(h\nu)$ was calculated as 1.493 eV. This value is 3.55% greater than the previously calculated electronic bandgap value [2].

In Fig. 3b), the maximum peak value of the imaginary part of the dielectric function $\varepsilon_2(\omega)$ for $CH_3NH_3Pb_{0.750}Ca_{0.250}I_3$ phase has shifted to the range 3–3.5 eV. However, the maximum peak start region does not change. The behavior of this region provides evidence of the usability of the zero-crossing point in calculating the optical bandgap of the $(\alpha h\nu)^2$-$(h\nu)$ graph. The optical bandgap is calculated as 1.537 eV. This result is very consistent with the electronic bandgap value (1.54 eV) [2].

Finally, details of the optical bandgap calculation of $CH_3NH_3Pb_{0.875}Sr_{0.125}I_3$, and $CH_3NH_3Pb_{0.750}Sr_{0.250}I_3$ non-stoichiometric crystal phases are given in Fig. 4 a) and Fig. b). Fig. 4a) shows the changes in the imaginary part of the dielectric function $\varepsilon_2(\omega)$ of the $CH_3NH_3Pb_{0.875}Sr_{0.125}I_3$ phase and the $(\alpha h\nu)^2$ term against the photon energy. The imaginary part of the dielectric function $\varepsilon_2(\omega)$ exhibits two large peaks at approximately 3 eV and 6.75 eV energies. These peaks are greater than the peak at 6.75 eV, around 3 eV. Also, the first peak with a maximum of 3 eV forms the beginning of the region where the optical band gap value of the crystal phase is calculated. The zero-crossing point of the $(\alpha h\nu)^2$-$(h\nu)$ plot obtained from these data was calculated to be 1.503 eV. This value is approximately 1.46% smaller than the calculated electronic bandgap value (1.525 eV) [2]. Similarly, as given in Fig. 4b), the optical bandgap of the $CH_3NH_3Pb_{0.750}Sr_{0.250}I_3$ phase was calculated

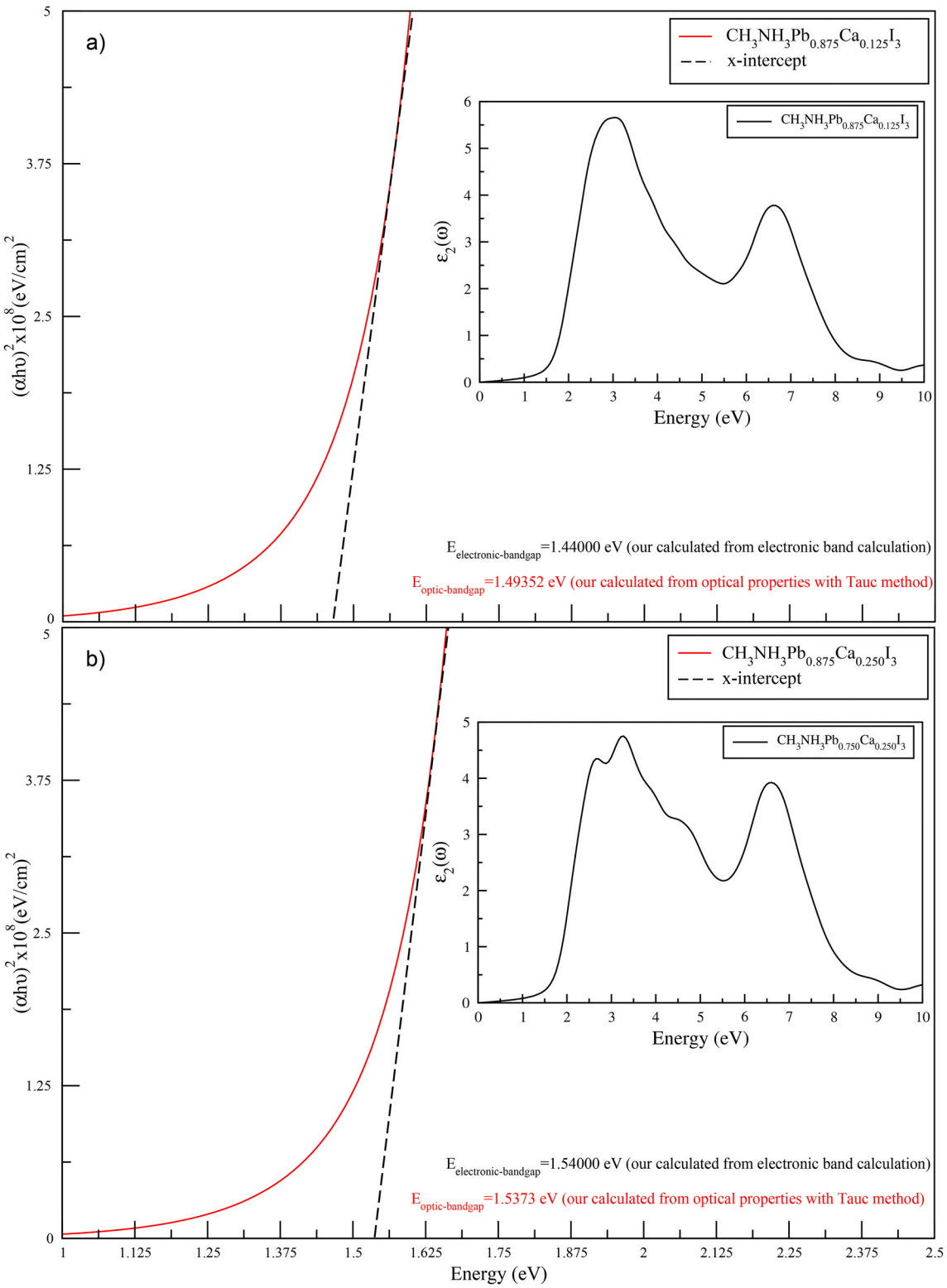

Fig. 3. The Tauc plot obtained using the zero-crossing point of the $(\alpha h\upsilon)^2$ versus $(h\upsilon)$. The right inset shows the imaginary part of the dielectric function $\varepsilon_2(\omega)$ in the non-stoichiometric a) $CH_3NH_3Pb_{0.875}Ca_{0.125}I_3$ and b) $CH_3NH_3Pb_{0.750}Ca_{0.250}I_3$ phases.

as 1.588 eV. There is a deviation of approximately 1.95% between the calculated optical bandgap and the electronic bandgap. Both bandgap values are calculated to be slightly higher than the expected value for ideal solar cells according to the SQ limit [21].

4. Conclusions

In this study, we computed the optical bandgaps (E_{opt-g}) of the $CH_3NH_3PbI_3$, $CH_3NH_3Pb_{0.875}Bi_{0.125}I_3$, $CH_3NH_3Pb_{0.875}Ca_{0.125}I_3$, $CH_3NH_3Pb_{0.750}Ca_{0.250}I_3$, $CH_3NH_3Pb_{0.875}Sr_{0.125}I_3$, and $CH_3NH_3Pb_{0.750}Sr_{0.250}$ I_3 perovskite crystal structures using optical arguments such as the

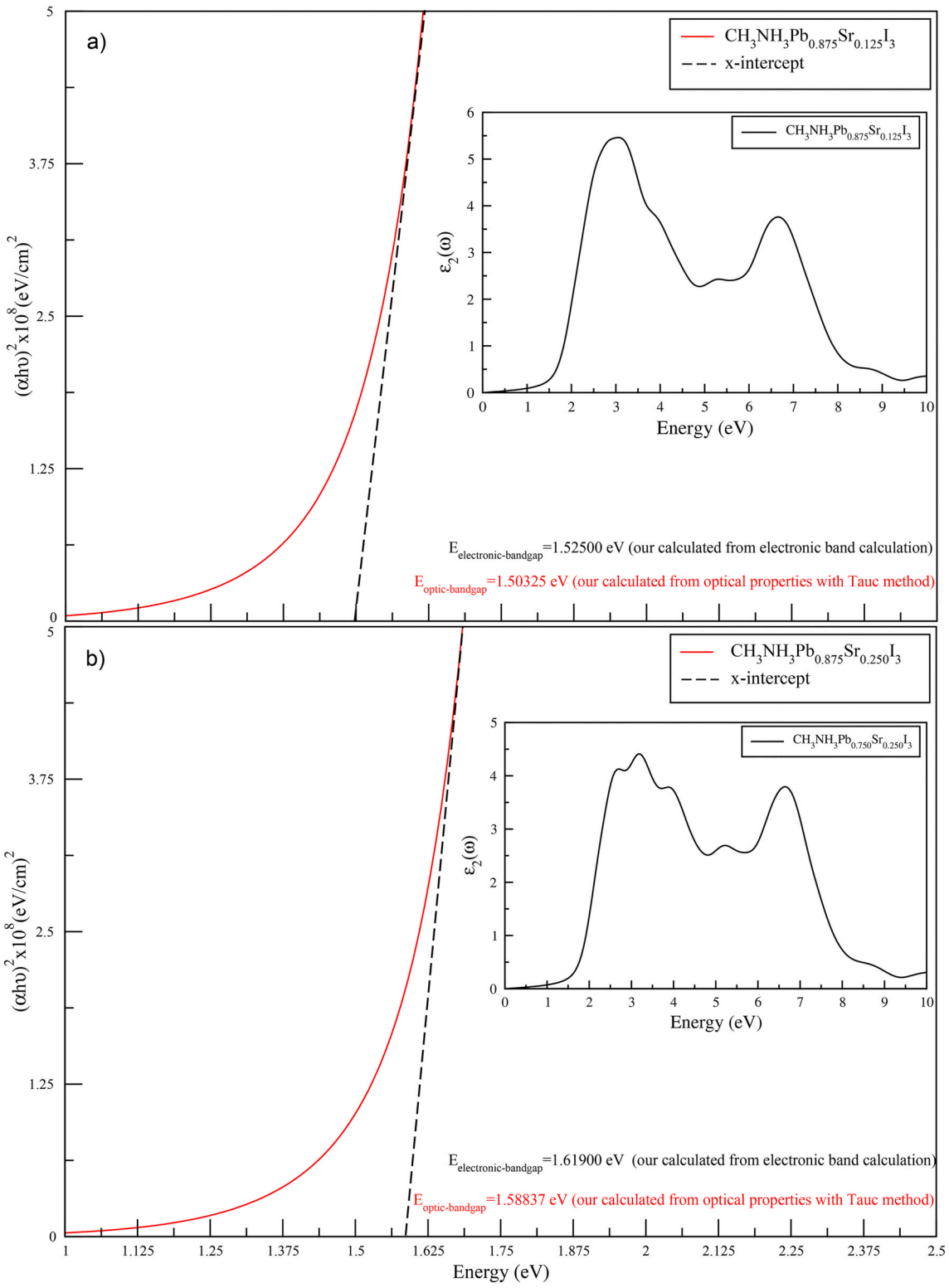

Fig. 4. The Tauc plot obtained using the zero-crossing point of the $(\alpha\hbar\upsilon)^2$ versus $(\hbar\upsilon)$. The right inset shows the imaginary part of the dielectric function $\varepsilon_2(\omega)$ in the non-stoichiometric a) $CH_3NH_3Pb_{0.875}Sr_{0.125}I_3$ and b) $CH_3NH_3Pb_{0.750}Sr_{0.250}I_3$ phases.

imaginary part of the dielectric function $\varepsilon_2(\omega)$, absorption coefficient (α), the zero-crossing point of the $(\alpha\hbar\upsilon)^2$ versus excitation photon energy $(\hbar\upsilon)$. We compared our results of the electronic bandgaps $(E_{elect-g})$ and optical bandgaps (E_{opt-g}) calculated in our previous studies.

The calculated optical bandgap (E_{opt-g}) as 1.694 eV for the stoichiometric $CH_3NH_3PbI_3$ crystal phase is very compatible with the electronic bandgap $(E_{elect-g})$ calculated as 1.682 eV in the previous study. The deviation is only 0.71%. Besides, the calculated optical bandgaps are also compatible with other experimental and theoretical studies.

We calculated the optical band gaps (E_{opt-g}) of non-stoichiometric $CH_3NH_3Pb_{0.875}Bi_{0.125}I_3$, $CH_3NH_3Pb_{0.875}Ca_{0.125}I_3$, $CH_3NH_3Pb_{0.750}Ca_{0.250}I_3$, $CH_3NH_3Pb_{0.875}Sr_{0.125}I_3$, and $CH_3NH_3Pb_{0.750}Sr_{0.250}$ I_3 perovskite crystal phases as 1.358 eV, 1.493 eV, 1.537 eV, 1.503 eV and 1.588 eV, respectively. The calculated electronic bandgaps ($E_{elect-g}$) for these phases in our previous study are 1.306 eV, 1.440 eV, 1.540 eV, 1.525 eV and 1.619 eV, respectively. When the calculated electronic and optical bandgaps are compared, it is seen that the results are in agreement. Besides, the optical band gaps (E_{opt-g}) were calculated for the non-stoichiometric $CH_3NH_3Pb_{(1-x)}Y_{(x)}I_3$ (Y=Bi, x = 0.125) and $CH_3NH_3Pb_{(1-x)}Y_{(x)}I_3$ (Y=Ca, Sr, x = 0.125, 0.250) phases are reported for the first time in this study. Therefore, there is no experimental or theoretical study by which we can compare our optical bandgap results. Hence, we think that our results will contribute to the literature for the non-stoichiometric crystal structures studied.

Credit author statement

Cengiz Soykan: Methodology, Writing-Original draft preparation, Visualization, Software. Hasan Gocmez: Supervision, Theory, Experimental control, Reviewing, and Editing.

Declaration of competing interest

The authors declare that they have no known competing financial interests or personal relationships that could have appeared to influence the work reported in this paper.

Acknowledgments

This study was supported by TUBITAK through project number 116F073. Theoretical computations are carried out on TUBITAK-ULAKBIM clusters. The authors would like to thank all who supported in carrying out this study.

References

[1] C. Soykan, H. Goçmez, The physical properties of bismuth replacement in lead halogen perovskite solar cells: $CH_3NH_3Pb_{1-x}Bi_xI_3$ compounds by ab-initio calculations, Results Phys 13 (2019) 102–278, https://doi.org/10.1016/j.rinp.2019.102278.

[2] C. Soykan, H. Goçmez, Comparison of the effects of Sr^{2+} and Ca^{2+} substitution on the structural and electronic properties of the perovskites $CH_3NH_3Pb_{1-x}Y_xI3$ (Y=Sr, Ca) by using the Density Functional Theory, Physica B (2021) 412579, https://doi.org/10.1016/j.physb.2020.412579.

[3] H.S. Kim, C.R. Lee, J.H. Im, K.B. Lee, T. Moehl, A. Marchioro, S.J. Moon, R. Humphry-Baker, J.H. Yum, J.E. Moser, M. Gratzel, N.G. Park, Lead iodide perovskite sensitized all-solid-state submicron thin film mesoscopic solar cell with efficiency exceeding 9% N.G. Park, Sci. Rep. 2 (2012) 591, https://doi.org/10.1038/srep00591.

[4] T. Baikie, Y. Fang, J.M. Kadro, M. Schreyer, F. Wei, S.G. Mhaisalkar, et al., Synthesis and crystal chemistry of the hybrid perovskite (CH3NH3)PbI3 for solid-state sensitized solar cell applications, J. Mater. Chem. 1 (2013), https://doi.org/10.1039/c3ta10518k, 5628–41.

[5] Y. Yamada, T. Nakamura, M. Endo, A. Wakamiya, Y. Kanemitsu, Near-band-edge optical responses of solution-processed organic-inorganic hybrid perovskite $CH_3NH_3PbI_3$ on mesoporous TiO2 electrodes, APEX 7 (2014), https://doi.org/10.7567/APEX.7.032302, 032302.

[6] Y. Dang, X. Tao, Y. Liu, Y. Sun, D. Yuan, X. Liu, et al., Bulk crystal growth of hybrid perovskite material $CH_3NH_3PbI_3$, RSC Pub. Cryst. Eng. Comm. (2013) 1–3, https://doi.org/10.1039/C4CE02106A, 00.

[7] J. Navas, A. Sánchez-Coronilla, J.J. Gallardo, J.C. Piñero, D. De los Santos, E. I. Martín, N.C. Hernández, R. Alcántara, C. Fernández-Lorenzo, J. Martín-Calleja, The impact of Pd on the light-harvesting in hybrid organic-inorganic perovskite for solar cells, Nanomater. Energy 34 (2017) 141–154, https://doi.org/10.1016/j.nanoen.2017.02.035.

[8] P. Hohenberg, W. Kohn, Inhomogeneous electron gas, Physiol. Rev. B 136 (1964) 864, https://doi.org/10.1103/PhysRev.136.B864.

[9] W. Kohn, L.J. Sham, Self-consistent equations including exchange and correlation effects, Phys. Rev. 140 (1965) 1133, https://doi.org/10.1103/PhysRev.140.A1133.

[10] W. Kohn, A.D. Becke, R.G. Parr, Density functional theory of electronic structure, J. Phys. Chem. 100 (1996) 974, https://doi.org/10.1021/jp960669l.

[11] G. Kresse, J. Furthmuller, Efficiency of ab-initio total-energy calculations for metals and semiconductors using a plane-wave basis set, Comput. Mater. Sci. 6 (1996) 15–50, https://doi.org/10.1016/0927-0256(96)00008-0.

[12] G. Kresse, J. Furthmuller, Efficient iterative schemes for ab-initio total-energy calculations using a plane-wave basis set, Phys. Rev. B 54 (1996) 11169, https://doi.org/10.1103/PhysRevB.54.11169.

[13] J. Hafner, Materials simulations using VASP a quantum perspective to materials science, Comput. Phys. Commun. 177 (2007) 6–13, https://doi.org/10.1016/j.cpc.2007.02.045.

[14] G. Kresse, J. Hafner, Ab initio molecular dynamics for liguid metals, Phys. Rev. B 47 (1993) 558, https://doi.org/10.1103/PhysRevB.47.558.

[15] G. Kresse, J. Hafner, Norm-conserving and ultrasokf pseudopotentials for first-row and transition elements, J. Phys. Condens. Matter 6 (1994) 8245, https://doi.org/10.1088/0953-8984/6/40/015.

[16] P.E. Blöchl, Projector augmented-wave method, Phys. Rev. B 50 (1994) 17953–17978, https://doi.org/10.1103/PhysRevB.50.17953.

[17] J.P. Perdew, K. Burke, M. Ernzerhof, Generalized gradient approximation made simple, Phys. Rev. Lett. 77 (1996) 3865, https://doi.org/10.1103/PhysRevLett.77.3865.

[18] A.M. Ganose, A.J. Jackson, D.O. Scanlon, sumo: command-line tools for plotting and analysis of periodic ab initio calculations, JOSS 3 (2018) 717, https://doi.org/10.21105/joss.00717, 28.

[19] H.J. Monkhorst, J.D. Pack, Special points for Brillouin-zone integrations, Phys. Rev. B 13 (1976) 5188–5192, https://doi.org/10.1103/PhysRevB.13.5188.

[20] N. Serpone, D. Lawless, R. Khairutdinov, sumo: command-line tools for plotting and analysis of periodic ab initio calculations, J. Phys. Chem. 99 (1995) 16646–16654, https://doi.org/10.1021/j100045a026, 45.

[21] W. Shockley, H.J. Queisser, Detailed balance limit of efficiency of p-n Junction Solar Cells, J. Appl. Phys. 32 (1961) 510, https://doi.org/10.1063/1.1736034.